A measurement method for the characterization of the ferromagnetic bottom layer of cookware used in domestic induction heating

1st Felix Rehm*, 2nd Patrick Breining, 3rd Marc Hiller
Elektrotechnisches Institut (ETI)
Karlsruhe Institute of Technology (KIT)
Karlsruhe, Germany
*E-mail: felix.rehm@kit.edu

***Abstract*—Design-oriented modeling approaches, such as finite element analyses (FEA), rely on accurate material data. However, manufacturers rarely provide the necessary data for cookware used in domestic induction heating. Due to the multi-layered structure of the cookware bottom, conventional measurement methods for the characterization of magnetic material are not applicable without great effort in preparation of suited material specimen. This contribution proposes a novel measurement method that allows determining the electromagnetic properties of the ferromagnetic bottom layer of cookware. The proposed measurement method is based on the minimization of deviation between measurement and simulation data in dependence of material properties. By characterization of the ferromagnetic bottom layer of a material specimen made from multiple layers, the feasibility of the method is shown. The results presented for the magnetic material characterization are validated using Epstein frame measurements. It is shown that the deviation between the magnetization curve determined with the proposed method and the tip of the hysteresis curve measured using the Epstein frame is approximately 3 %. To validate the results presented for the specific electrical resistance, a microhmmeter is used. The relative error between both measurements is approximately 16 %.**

***Index Terms*—domestic induction heating, load modeling, nonlinear simulation, material characterization**

I. Introduction

In domestic appliances, induction heating (IH) has become increasingly popular in recent years due to its efficiency, cleanliness and fast heating [1]. Compared to classical heating methods such as resistance heating or gas stoves, the heat is generated directly within the cookware to be heated.

Fig. 1 schematically shows the cross section of the electromagnetic part of an IH system. It can be seen that the cookware to be heated, e.g. a pot, is placed above the induction coil, which is separated through a glass-ceramic from the ferromagnetic bottom of the cookware. The induction coil, consisting of spiral wound litz wire and ferrite material, generates an alternating magnetic field in the frequency range of $20\,\mathrm{kHz} - 100\,\mathrm{kHz}$ [2]. Consequently, eddy currents as well as magnetic hysteresis losses generate heat in the ferromagnetic material of the pot. As the efficiency of an IH system depends on the electromagnetic properties of the material to be heated, knowledge about these properties is necessary during the design process [3].

To describe the behaviour of the electromagnetic part of an IH system, different models can be used. The modeling approach given in [4] makes use of a nonlinear passive network, which consists of frequency-dependent and frequency-independent components. The simplest model is a series connection of an equivalent inductor L_{eq} and an equivalent resistor R_{eq} as shown in Fig. 2 [5], [6]. Additionally, the dependency of L_{eq} and R_{eq} on the electrical frequency f and the amplitude of the inductor current i_{L} is taken into account in [2].

A convenient way to determine the values of L_{eq} and R_{eq} is through measurements as done in [7]. A measurement testbench was developed to accurately measure different inductor-pot combinations. This approach allows to determine the equivalent impedance of an inductor-pot combination without any knowledge about the nonlinear magnetic properties of the ferromagnetic materials used. Alternatively, parametrization of a model can be performed using simulation data. If finite element analyses (FEA) are used, accurate data about geometrical and physical properties of the system are required. For instance, the geometrical structure of the cookware bottom can be determined using cut samples (Fig. 3). However, manufacturers rarely provide detailed information about electromagnetic material properties. To overcome this problem, special material specimen made of ferromagnetic steel were characterized using a Single Sheet Tester (SST) in [2].

Nevertheless, due to the structure of the cookware bottom, conventional measurement methods used for the characterization of magnetic material, such as SST, Epstein frame or ring

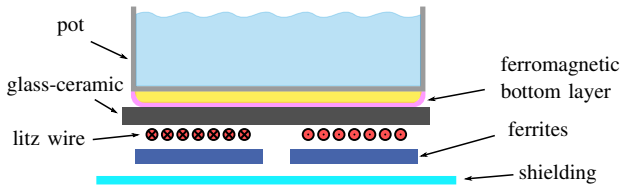

Fig. 1: Schematic of the cross section of the electromagnetic part of an IH system.

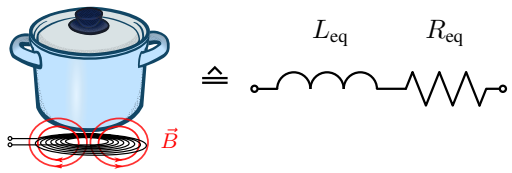

Fig. 2: Equivalent impedance model of the coupled inductor-pot system.

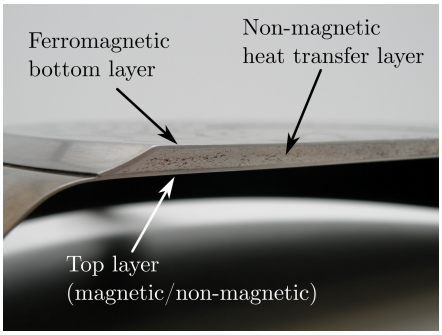

Fig. 3: Cross section of the bottom of cookware with different material layers shown.

core measurements are not applicable for the characterization of the ferromagnetic material layer of already manufactured cookware. The aforementioned methods need test specimen, which consist only of the material to be characterized [8]. For the characterization of already manufactured IH cookware, this would result in great effort to separate the different material layers.

Therefore, a novel measurement method is introduced, which allows the characterization of the electromagnetic properties of the ferromagnetic bottom layer of cookware used in domestic IH. For use of the proposed method, preparation of special material specimen is not required. Only the height of the different material layers need to be measured in advance. This can, for instance, be done using cut samples or computed tomography scan.

II. Measurement Method

In the following, the measurement principle will be discussed and the simulation setup will be shown. It is assumed, that the top layer of the material specimen is made of the same ferromagnetic material as the bottom layer and the heat transfer layer is made of copper.

The measurement principle is based on the measurement of the resulting magnetic flux ϕ_2 in a given magnetic resistance network consisting of $R_{\text{m,Yoke}}$, $R_{\text{m,Pot}}$, $R_{\sigma,\text{Yoke}}$ and $R_{\sigma,\text{Pot}}$ according to Fig. 4. Therein $R_{\text{m,Pot}}$ denotes the magnetic resistance of the ferromagnetic bottom layer of the pot and $R_{\text{m,Yoke}}$ the magnetic resistance of the yoke, designed as a P-Type ferrite core with known parameters. $R_{\sigma,\text{Yoke}}$ and $R_{\sigma,\text{Pot}}$ denote the magnetic resistances of the stray paths, which are neglected in the following. Fig. 5 shows that two coils are inserted into the ferrite core. The primary coil is connected to the output stage of a linear amplifier and is responsible for the excitation of the magnetic circuit. The excitation can

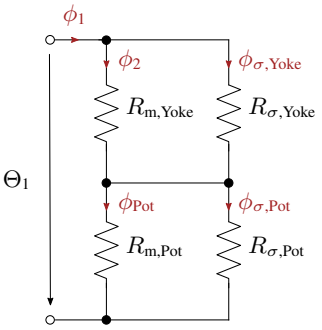

Fig. 4: Magnetic circuit of the measurement setup with source of excitation Θ_1 and resulting flux ϕ_1 in resistance network.

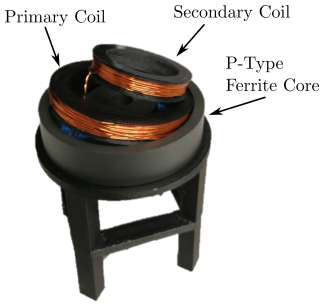

Fig. 5: P-type ferrite core with outer diameter of $d_{\text{f,o}} = 69\,\text{mm}$ as well as primary and secondary coils shown.

be calculated through $\Theta_1 = n_1 \cdot i_1$, where n_1 is the number of turns in the primary coil and i_1 the associated current. Neglecting the stray flux within the magnetic circuit results in $\phi_1 = \phi_2 = \phi_{\text{Pot}}$. Then, (1) shows, that in dependence of the excitation Θ_1 and the values of the magnetic resistances $R_{\text{m,Yoke}}$ and $R_{\text{m,Pot}}$, a magnetic flux ϕ_2 is present in the magnetic circuit.

$$\phi_2 = \frac{\Theta_1}{R_{\text{m,Yoke}} + R_{\text{m,Pot}}} \tag{1}$$

For a given current i_1, a voltage $v_2 = n_2 \cdot \frac{\mathrm{d}\phi_2}{\mathrm{d}t}$ can be measured at the terminals of the secondary coil, whose number of turns is denoted by n_2. Due to the relatively large distance between the ferromagnetic top and bottom layers, they are magnetically isolated from each other. If the properties of the magnetic yoke $R_{\text{m,Yoke}}$ are well-known, the resulting flux ϕ_2 only depends on the material properties of the ferromagnetic bottom layer of the pot $R_{\text{m,Pot}}$, which is placed on top of the ferrite core.

At the test bench different operating points, defined by the amplitude and the electrical frequency f of the primary current i_1 are measured. However, a detailed discussion of the test bench is not part of this contribution, further information is given in [9].

A. Determination of magnetic properties

To determine the magnetic material properties of the bottom layer, the error between measurement and simulation results is minimized using a constraint nonlinear optimization algorithm. Herein, the objective function J_{obj} to be minimized with respect to the magnetic material parameters is defined as

$$J_{\text{obj}} = \sum_{i=1}^{N} (\Psi_{2,\text{m}}(t_i) - \Psi_{2,\text{s}}(t_i))^2 + (\hat{B}_{\text{m}} - \hat{B}_{\text{s}})^2, \tag{2}$$

with N being the number of simulated time steps within a period. $\Psi_{2,x}(t_i)$ describes the value of flux-linkage at the time step t_i, with $\Psi_{2,x}(t_i) = n_2 \cdot \phi_{2,x}(t_i)$. $\hat{B}_x$ denotes the maximum value of the flux density in point P_1, which occurs in the bottom layer of the pot as shown in Fig. 6. The values are either taken from measurement ($x \equiv$ m) or simulation data ($x \equiv$ s). Simulations are carried out in terms of two-dimensional transient FEA simulations for the geometry shown

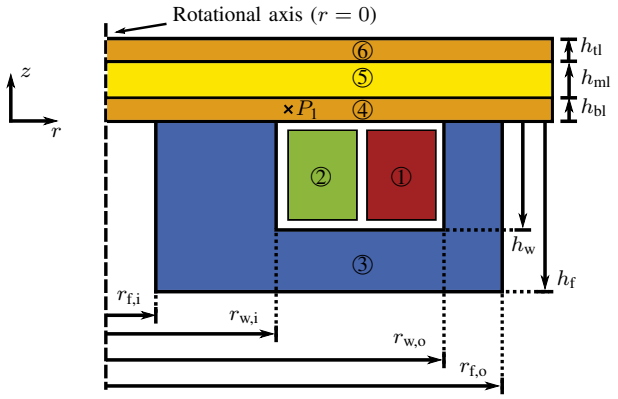

Fig. 6: Schematic of rotational symmetric simulation model with primary coil ①, secondary coil ②, ferrite core ③ and material specimen, which consists of a ferromagnetic bottom layer ④, a non-magnetic heat transfer layer ⑤ and a ferromagnetic top layer ⑥.

in Fig. 6. The rotational symmetric simulation model consists of the ferrite core, the primary and secondary coils as well as the material specimen. For the specific measurement setup shown in Fig. 6, the coordinates of $P_1(r_1|z_1)$ are empirically determined such that the magnitude of the flux density $|\vec{B}|$ is independent of the height z. Fig. 7 shows the magnitude of the flux density $|\vec{B}|$, as well as its radial and axial components (B_r and B_z) within the ferromagnetic bottom layer in dependence of the height z for $r = r_{w,i}$ and $r = r_{w,i} + 1\,\mathrm{mm}$. As shown in Fig. 7a, the magnitude of the flux density $|\vec{B}|$ at $r = r_{w,i}$ and $z = 0$ is approximately $0.6\,\mathrm{T}$ higher than it is for $z = h_{bl}$. Evaluating the flux density for different values of z leads to varying results regarding (2). To overcome this problem and assure that $|\vec{B}|$ is independent of z, r_1 is chosen to be $r_{w,i} + 1\,\mathrm{mm}$. As shown in Fig. 7b, $|\vec{B}|$ is independent of the height z for $r = r_{w,i} + 1\,\mathrm{mm}$, such that the choice of z_1 does not affect the function value of (2).

Within the FEA software package *"Altair Flux 2021"*, the magnetic properties of the ferromagnetic material layer is modeled by the analytic description given through

$$B(H) = \mu_0 H + J_s \cdot \frac{H_a + 1 - \sqrt{(H_a+1)^2 - 4H_a(1-\alpha)}}{2(1-\alpha)} \tag{3}$$

with

$$H_a = \mu_0 H \cdot \frac{\mu_r - 1}{J_s}, \tag{4}$$

μ_0 as the permeability of vacuum, μ_r as the initial relative permeability, J_s as the magnetic polarization at saturation and α as adjustment coefficient [10].

Fig. 8 demonstrates the influence of the material parameters on the shape of the magnetization curve. As shown in Fig. 8a, the initial relative permeability μ_r has a major influence on the shape of the magnetization curve in the linear section at a low field strength H, while it has less influence at high values of H, where saturation occurs. According to Fig. 8b, the parameter J_s has a major influence for high values of H and minor influence for small values of the field strength. The adjustment factor α influences the bending of the magnetization curve in the range between the linear section and the section where saturation occurs (Fig. 8c).

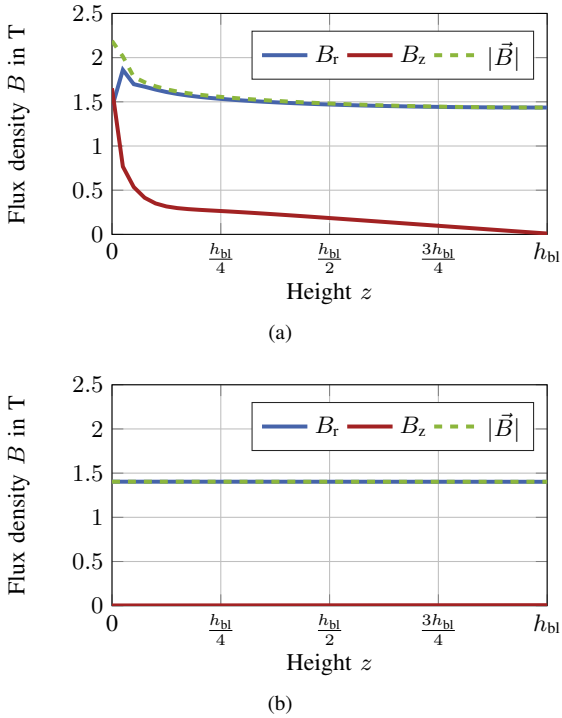

Fig. 7: Magnitude as well as radial and axial components of flux density $\vec{B}$ in dependence of height z in the ferromagnetic bottom layer for $f = 10\,\mathrm{Hz}$ at (a) $r = r_{w,i}$ and (b) $r = r_{w,i} + 1\,\mathrm{mm}$.

B. Determination of electrical properties

The electrical properties of the ferromagnetic layer are defined by the specific electrical resistance ρ. At operating points with low frequency f, the eddy current in the pot bottom and therefore the opposing field strength is negligible. The eddy current increases at higher frequencies, which results in a stronger opposing field strength. Therefore, the specific electrical resistance ρ has a greater influence on the resulting flux-linkage Ψ_2 for high frequencies than it has for low frequencies. This is exemplarily shown in Fig. 9 for the same current amplitude of i_1 at frequencies of $10\,\mathrm{Hz}$ and $1500\,\mathrm{Hz}$. To assure that saturation occurs within the ferromagnetic material layer, the amplitude of i_1 is chosen such that the shape of i_1 becomes non-sinusoidal. Fig. 9 shows an exemplary non-sinusoidal shape of i_1, which will be referred to as nonlinear operating points in the following.

Additionally, at higher frequencies the skin effect causes an in-homogeneous field distribution within the bottom layer. Fig. 10 shows the magnitude $|\vec{B}|$ as well as the radial and axial components of the flux density at $r = r_{w,i} + 1\,\mathrm{mm}$. It is obvious, that contrarily to Fig. 7b, the flux density is not constant over the height of the ferromagnetic bottom layer. For determination of the specific electrical resistance ρ the objective function J_{obj}, which is minimized with respect to ρ,

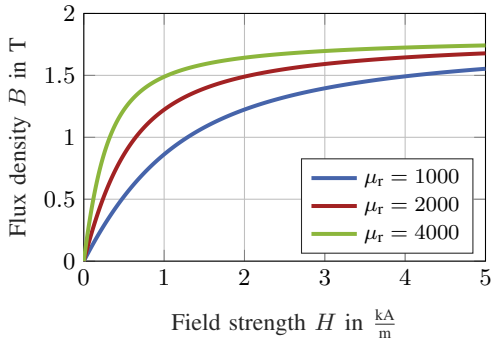

(a)

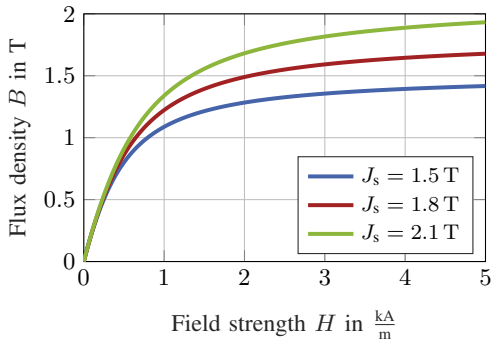

(b)

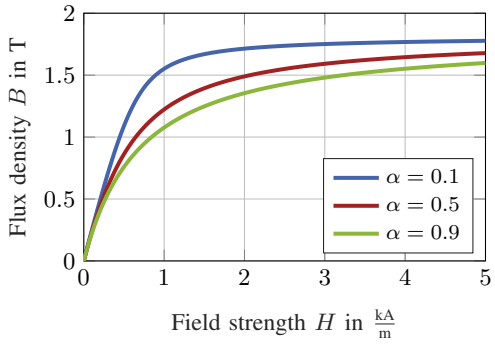

(c)

Fig. 8: Magnetization curves described by (3) for different combinations of parameters with reference values (red curves) of $\mu_\text{r} = 2000$, $J_\text{s} = 1.8\,\text{T}$ and $\alpha = 0.5$ with (a) variation of μ_r, (b) variation of J_s and (c) variation of α.

is therefore chosen to be

$$J_\text{obj} = (\hat{\Psi}_\text{2,m} - \hat{\Psi}_\text{2,s})^2. \tag{5}$$

In conclusion, to separate the influence of the magnetic and the electrical properties of the material specimen, we propose to measure operating points at low and high frequencies. The magnetic properties of the material are determined at low frequencies and once these are known, the electrical properties are determined at high frequencies. The resulting workflow for the characterization of a material specimen is given in Fig. 11.

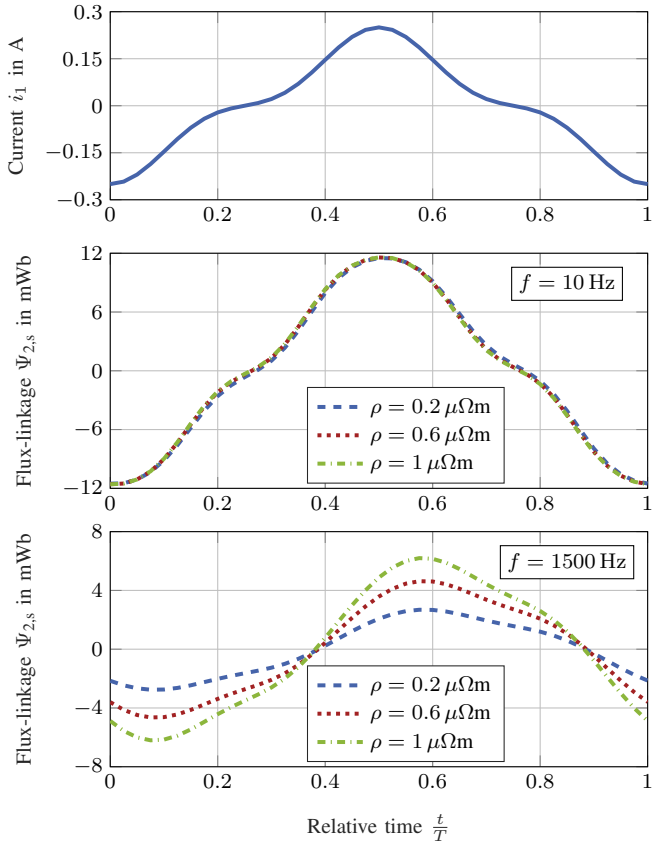

Fig. 9: Simulation results of flux-linkage in secondary coil for a nonlinear operating point at $f = 10\,\text{Hz}$ and $f = 1500\,\text{Hz}$ for varying specific electrical resistance ρ. The magnetic properties of the material specimen are defined as $\mu_\text{r} = 1000$, $J_\text{s} = 1.8\,\text{T}$ and $\alpha = 0.5$.

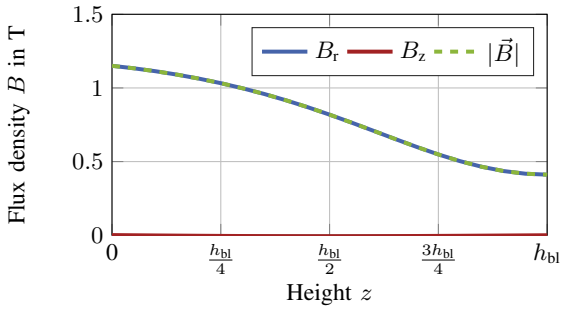

Fig. 10: Magnitude as well as radial and axial component of flux density $\vec{B}$ in dependence of height z in the ferromagnetic bottom layer at $r = r_\text{w,i} + 1\,\text{mm}$ for $f = 1500\,\text{Hz}$.

III. Experimental Results

A. Determination of magnetic properties

To demonstrate the feasibility of the proposed measurement method, material specimen consisting of three material layers are used. While the bottom and top layers are made of ferromagnetic stainless steel of type 1.4016 (AISI 430), the nonmagnetic heat transfer layer is made of copper. Measurements are performed for a nonlinear operating point at a frequency of $f = 10\,\text{Hz}$. The number of turns in the primary and secondary

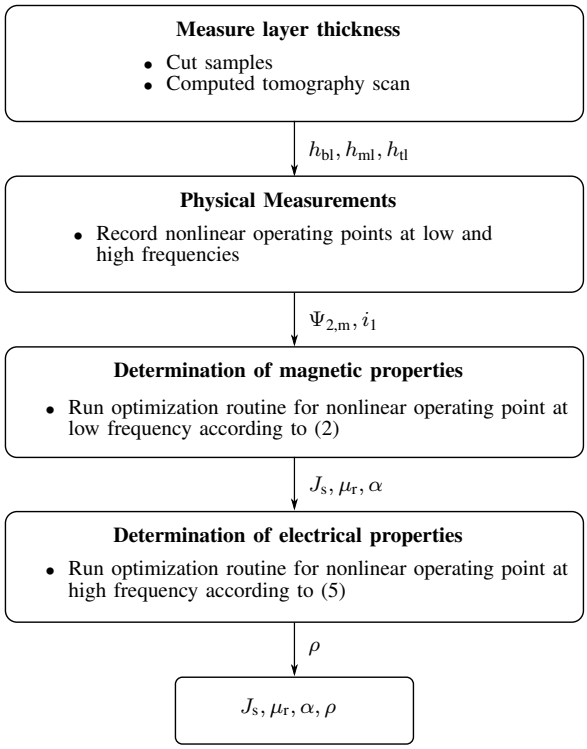

Fig. 11: Resulting workflow of proposed measurement method with different steps and output variables.

coils are $n_1 = 110$ and $n_2 = 100$, respectively. The remaining geometrical and physical parameters of the measurement setup are given in Table I. Fig. 6 shows the corresponding simulation model.

The measurement results of the primary current i_1 and the flux-linkage $\Psi_{2,m}$ (blue curves in Fig. 12) are used as input variables for the optimization routine. The flux-linkage $\Psi_{2,s}$, resulting after the minimization of the objective function J_{obj} given through (2), is shown in Fig. 12b. It can be seen, that a deviation between measurement and simulation results exists, especially in between the two maxima at $t_1 = 30\,\mathrm{ms}$ and $t_2 = 80\,\mathrm{ms}$. The mismatch of both graphs reaches its maximum in the zero-crossings of i_1. This error is caused by the analytical model of the magnetization curve given through (3), which does not take magnetic hysteresis into account. Fig. 13 shows the hysteresis curve of the ferromagnetic material, whose coercive force is $H_c = 672\,\mathrm{Am}^{-1}$ and the remanent flux density is $B_r = 0.63\,\mathrm{T}$. Therefore, in the graphs of measurement and simulation results a deviation regarding the flux-linkage Ψ_2 occurs. Nevertheless, as the red curve in Fig. 13 shows, the determined magnetization curve is within the bounds given by the hysteresis curve and shows a deviation of less than $45\,\mathrm{mT}$ at the maximum value of $1.2\,\mathrm{T}$ of the hysteresis curve. The resulting parameters describing the magnetization curve given through (3) are: $J_s = 1.35\,\mathrm{T}$, $\mu_r = 1419.6$ and $\alpha = 0.58$.

TABLE I: Geometrical and physical parameters of measurement setup.

Parameter	Value	
$r_{f,i}$	4.3	mm
$r_{w,i}$	14.7	mm
$r_{w,o}$	29.2	mm
$r_{f,o}$	34.5	mm
h_w	9.1	mm
h_f	14	mm
h_{bl}	0.78	mm
h_{ml}	2	mm
h_{tl}	0.78	mm
$\mu_{r,ferrite}$	2300	

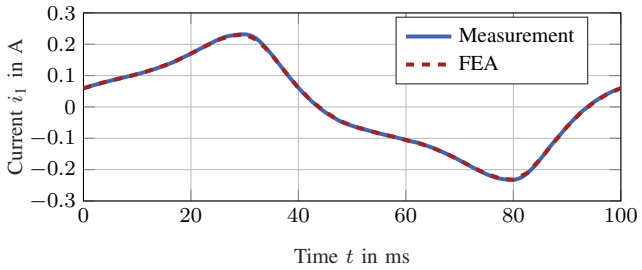

(a) Excitation current i_1

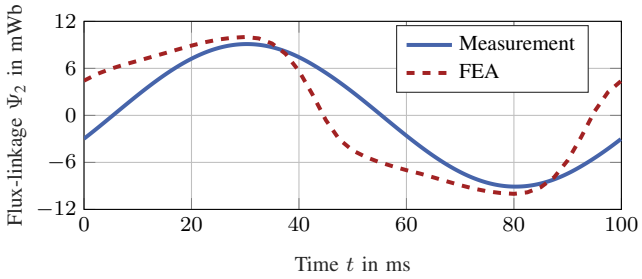

(b) Resulting flux-linkage Ψ_2

Fig. 12: Excitation current i_1 and resulting flux-linkage Ψ_2 for measurement (blue curve) and output of optimization routine (red curve) at $f = 10\,\mathrm{Hz}$.

B. Determination of electrical properties

For the same material specimen measurements are performed at a frequency of $f = 1500\,\mathrm{Hz}$ to determine the specific electrical resistance ρ. The number of turns in the primary and secondary coils are $n_1 = 25$ and $n_2 = 20$, respectively. According to the previous results, the magnetic properties are defined as $J_s = 1.35\,\mathrm{T}$, $\mu_r = 1419.6$ and $\alpha = 0.58$ and the objective function J_{obj} given in (5) is minimized with respect to ρ. Fig. 14 shows the graphs for measurement and simulation results after running the optimization routine. The amplitudes of the flux-linkage match for both measurement and simulation, while there is a deviation in the time interval between the maxima. As described before, this error is caused by the analytic expression used to model the magnetic properties of the ferromagnetic material and not taking hysteresis effects into account.

The stopping criterion of the optimization routine is reached at a value of $\rho_{sim} = 475 \times 10^{-9}\,\Omega\,\mathrm{m}$. To validate this re-

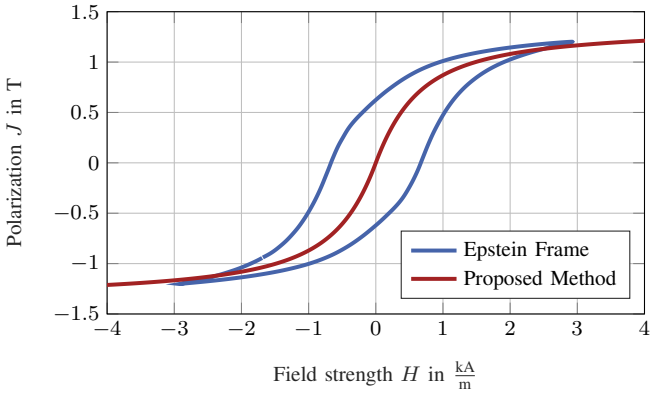

Fig. 13: Magnetization curve determined with proposed method (red curve) and hysteresis curve measured using an Epstein Frame (blue curve).

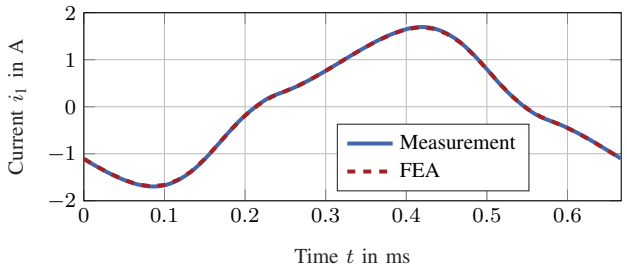

(a) Excitation current i_1

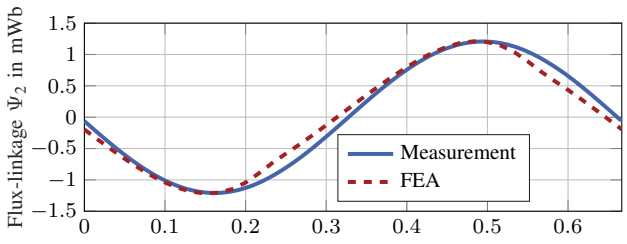

(b) Resulting flux-linkage Ψ_2

Fig. 14: Excitation current i_1 and resulting flux-linkage Ψ_2 for measurement (blue curve) and output of optimization routine (red curve) at $f = 1500\,\text{Hz}$. The magnetic properties are: $J_\text{s} = 1.35\,\text{T}$, $\mu_\text{r} = 1419.6$ and $\alpha = 0.58$.

sult, additional measurements are performed using a *"Sefelec MGR10"* microhmmeter and a solid rectangular material specimen with a length $l = 100\,\text{mm}$, a width $w = 30\,\text{mm}$ and a height $h = 0.78\,\text{mm}$. With

$$\rho_\text{conv} = R \cdot \frac{w \cdot h}{l} \tag{6}$$

the specific electrical resistance ρ_conv can be calculated. For a measured resistance value of $R = 2.42\,\text{m}\Omega$, the specific electrical resistance becomes $\rho_\text{conv} = 566.3 \times 10^{-9}\,\Omega\,\text{m}$. The error between both values is approximately 16 %.

IV. Conclusion

In this contribution, we propose a novel measurement method to determine electromagnetic material properties of cookware used in domestic IH. The feasibility of the method is demonstrated on a multi-layered material specimen and the results are compared to measurements using conventional methods. Applied to multi-layered material specimen the proposed method needs less effort in preparation of suitable material specimen compared to conventional measurement methods.

For determination of magnetic material properties, the measured and simulated graphs of flux-linkage show a deviation which reach a maximum in the zero-crossings. Nevertheless, the deviation between the magnetization curve determined with the proposed method and the hysteresis curve measured using an Epstein frame is approximately 3 % at the tip of the hysteresis curve.

Regarding the determination of the specific electrical resistance ρ, the proposed method is less accurate. The value determined differs by approximately 16 % from the value determined using a microhmmeter.

Still, the presented results can be used to model electromagnetic material properties, for instance for use in FEA simulations during the design process of an IH system. Subsequently the inaccuracy of FEA results, introduced by unknown electromagnetic properties of the pot bottom, can be reduced.

For our future work, we aim to improve the accuracy of the method by using different models to describe the magnetic properties and thereby consider magnetic hysteresis.

References

[1] O. Lucia, P. Maussion, E. J. Dede, and J. M. Burdio, "Induction Heating Technology and Its Applications: Past Developments, Current Technology, and Future Challenges," *IEEE Transactions on Industrial Electronics*, vol. 61, no. 5, pp. 2509–2520, May 2014.

[2] J. Serrano, J. Acero, I. Lope, C. Carretero, J. Burdio, and R. Alonso, "Modeling of domestic induction heating systems with non-linear saturable loads," in *2017 IEEE Applied Power Electronics Conference and Exposition (APEC)*. Tampa, FL, USA: IEEE, Mar. 2017, pp. 3127–3133.

[3] J. Acero, C. Carretero, I. Millan, R. Alonso, O. Lucia, and J. M. Burdio, "Experimental setup for inductive efficiency measurements of domestic induction systems based on energy balance," in *IECON 2010 - 36th Annual Conference on IEEE Industrial Electronics Society*. Glendale, AZ, USA: IEEE, Nov. 2010, pp. 114–119.

[4] D. Puyal, C. Bernal, J. M. Burdio, I. Millan, and J. Acero, "A new dynamic electrical model of domestic induction heating loads," in *2008 Twenty-Third Annual IEEE Applied Power Electronics Conference and Exposition*. Austin, TX, USA: IEEE, Feb. 2008, pp. 409–414.

[5] W. Hurley and M. Duffy, "Calculation of self and mutual impedances in planar magnetic structures," *IEEE Transactions on Magnetics*, vol. 31, no. 4, pp. 2416–2422, Jul. 1995.

[6] W. Hurley and M. Duffy, "Calculation of self- and mutual impedances in planar sandwich inductors," *IEEE Transactions on Magnetics*, vol. 33, no. 3, pp. 2282–2290, May 1997.

[7] D. Puyal, C. Bernal, J. M. Burdio, J. Acero, and I. Millan, "Methods and procedures for accurate induction heating load measurement and characterization," in *2007 IEEE International Symposium on Industrial Electronics*. Vigo, Spain: IEEE, Jun. 2007, pp. 805–810.

[8] *Magnetic materials Part 2: Methods of measurement of the magnetic properties of electrical steel strip and sheet by means of an Epstein frame (IEC 60404-2:1996 + A1:2008)*, European Committee for Electrotechnical Standardization.

[9] M. Veigel, P. Winzer, J. Richter, and M. Doppelbauer, "New FPGA-based and inline-capable measuring method for the identification of magnetic losses in electrical steel," p. 6.

[10] *User's Manual FEA software package "Altair Flux 2021"*, Altair Engineering Inc.